SCIENTIFIC REPORTS

OPEN

Received: 06 May 2016
Accepted: 26 January 2017
Published: 08 March 2017

Anisotropic layered Bi_2Te_3-In_2Te_3 composites: control of interface density for tuning of thermoelectric properties

Dongmei Liu[1], Xinzhong Li[2], Pedro Miguel de Castro Borlido[3], Silvana Botti[3], Roland Schmechel[4] & Markus Rettenmayr[1,5]

Layered $(Bi_{1-x}In_x)_2Te_3$-In_2Te_3 ($x = 0.075$) composites of pronounced anisotropy in structure and thermoelectric properties were produced by zone melting and subsequent coherent precipitation of In_2Te_3 from a $(Bi_{1-x}In_x)_2Te_3$ ($x > 0.075$) matrix. Employing solid state phase transformation, the Bi_2Te_3/In_2Te_3 interface density was tuned by modifying the driving force for In_2Te_3 precipitation. The structure-property relationship in this strongly anisotropic material is characterized thoroughly and systematically for the first time. Unexpectedly, with increasing Bi_2Te_3/In_2Te_3 interface density, an increase in electrical conductivity and a decrease in the absolute Seebeck coefficient were found. This is likely to be due to electron accumulation layers at the Bi_2Te_3/In_2Te_3 interfaces and the interplay of bipolar transport in Bi_2Te_3. Significantly improved thermoelectric properties of Bi_2Te_3-In_2Te_3 composites as compared to the single phase $(Bi_{1-x}In_x)_2Te_3$ solid solution are obtained.

Research on thermoelectrics has witnessed a renewal of interest with the drastic improvement of thermoelectric properties owing to nanoscaled structures, e.g. in thin film superlattice/quantum well multilayered structures[1–3]. Although the drawbacks of thin film materials such as their small scale, high cost and processing difficulties restrict their practical application, their favorable properties have stimulated extensive research on preparing nanostructured materials by bulk processes. Examples are high temperature high pressure pressing or spark plasma sintering of nanoscale powder[4,5]. Nanostructured materials prepared by bulk processes, which either contain nanometer sized grains or nanoscale precipitates, have been shown to exhibit a strongly enhanced thermoelectric performance. It is widely accepted that the enhancement is due to a high density of interfaces such as grain boundaries and heterophase interfaces[6–9]. Under certain conditions, the interfaces in thermoelectric materials augmented the Seebeck coefficient and reduced thermal and electrical conductivity by energy filtering of charged carriers[10]. Interfaces have on the other hand been found to induce an increase in electrical conductivity by selective scattering of lower mobility charged carriers by interfacial charged defects[11]. The questions how the interface density on the nanoscale can be controlled and how it affects the transport properties are challenging from both the engineering and the scientific viewpoint.

Several traditional metallurgical methods have shown their potential to achieve nanoscaled structures and to generate interfaces that are beneficial for the thermoelectric properties[12–21]. Physical processes such as eutectic reaction[12–15], solid state precipitation[16–19], and spinodal decomposition[20,21] have been exploited favorably and reproducibly. For clarifying structure-property relationships, the microstructural length scales can be varied systematically in a wide range by adjusting the processing parameters. For example, the lamellar spacing of the layered structure of PbTe and Sb_2Te_3 formed by the decomposition of $Pb_2Sb_6Te_{11}$ is controlled by the temperature and time of the decomposition process[16] and has been found to range from 30 nm at 200 °C to 200 nm at 500 °C.

[1]Otto Schott Institute of Materials Research, Friedrich Schiller University Jena, Löbdergraben 32, D-07743 Jena, Germany. [2]School of Materials Science and Engineering, Harbin Institute of Technology, West Da-Zhi Street 92, 150001 Harbin, China. [3]Institute for Condensed Matter Theory and Optics, Friedrich Schiller University Jena, Max-Wien-Platz 1, 07743 Jena, Germany. [4]Institute of Technology for Nanostructures and CENIDE, University of Duisburg-Essen, Bismarkstraße 81, 47057 Duisburg, Germany. [5]Center for Energy and Environmental Chemistry, Philosophenweg 7, D-07743 Jena, Germany. Correspondence and requests for materials should be addressed to M.R. (email: m.rettenmayr@uni-jena.de)

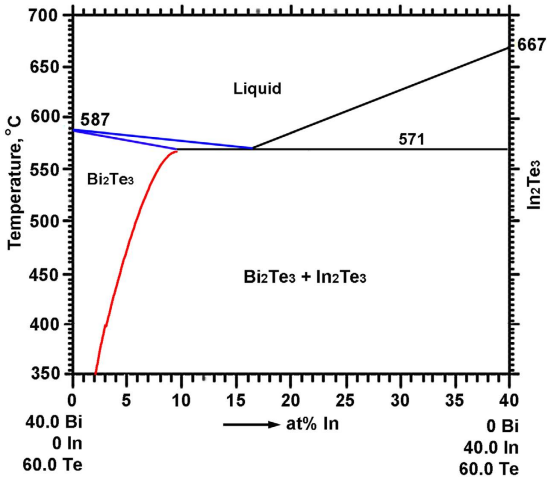

Figure 1. Pseudo-binary Bi_2Te_3-In_2Te_3 phase diagram[17,22,23]. The blue lines illustrate the recently reported solidus and liquidus lines[22], and the red line illustrates the recently reported solvus line of In in Bi_2Te_3 from ref. 17.

Up to present, the characterization of thermoelectric properties of lamellar thermoelectric materials generated by solidification/solid state phase transformation is either utterly lacking or carried out for isotropic materials prepared by conventional solidification processes. Recalling that lamellar structures formed via liquid/solid or solid state phase transformations exhibit preferential crystallographic orientations with respect to each other, a systematic analysis of the structure-property relationships should include the effects of anisotropy, and precise control of the lamellar growth direction should be attained in such materials, as e.g. by employing directional solidification techniques. In the present work, we apply a specially developed zone melting technique on Bi_2Te_3-In_2Te_3 samples, controlling the crystal orientation of the parent solid solution and the lamellar structure that is formed by solid state precipitation. The lamellar spacing is adjusted in a wide range by varying the supersaturation of the parent solid solution. Thoroughly characterized microstructural parameters are correlated with the thermoelectric performance for the first time. Suppression of bipolar transport and enhanced interface density contributed to an improved performance of the material.

Experimental

Synthesis. Oriented $(Bi,In)_2Te_3$ (containing 3, 4, 6, and 7.5 at%In) solid solutions with the {001} plane being parallel to the growth axis were obtained by a seeding zone melting technique[22]. This technique yields an especially uniform composition over the entire length of the zone melted region along the growth direction. More details on the control of macroscopic homogeneity via seeding zone melting can be found in ref. 22. Macroscopic homogeneity is a necessary precondition for the homogeneous distribution of precipitates and thus for a uniform thermoelectric performance of the bulk composite samples. The driving force for precipitation is temperature and concentration dependent, as can bee directly seen in the pseudo-binary Bi_2Te_3-In_2Te_3 phase diagram according to previous work in the literature[17,23] and our present work (Fig. 1). The blue lines illustrate the recently reported solidus and liquidus lines[22], based on which the concentration of the seed alloy for the seeding zone melting is selected. The seed alloys for 3, 4, 6 and 7.5 at% are 7, 9, 12.5 and 13.5 at%In, respectively.

Samples with In concentrations of 4, 6 and 7.5 at% were vacuum sealed in quartz and isothermally annealed for the precipitation of In_2Te_3. Note that homogenization after seeding zone melting is not necessary, as a perfectly homogeneous crystal is generated. This reduces possible artifacts and the misinterpretation of measured values significantly. Considering the temperature dependent solubility of In in Bi_2Te_3, as illustrated by the red line in Fig. 1, a uniform annealing temperature (400 °C in the present work) was chosen for all samples, resulting in a uniform and identical In concentration in the Bi_2Te_3 matrix in all samples, but a different Bi_2Te_3/In_2Te_3 interface density. After annealing for 6 days, the sample was water quenched. Annealing for a longer time of up to 12 days was also performed, but no further change in microstructure and thermoelectric properties was observed. This confirms that 6 days are long enough to reach the equilibrium. The microstructure consists of micro-/nanoscaled $\mathbf{Bi_2Te_3}/\mathbf{In_2Te_3}$ ("BTIT") lamellae of different spacing, depending on the initial In concentration. For simplification, all the BTIT composites are termed as BTIT-c with the initial In concentration c = 4, 6, 7.5, in at%In.

Materials characterization. The samples were prepared metallographically by grinding with a series of SiC papers up to a grit size of 4000, by polishing with 3 μm and 1 μm Al_2O_3 powder suspension, and finally polishing with 50 nm colloidal silica. The microstructure was observed using a scanning electron microscope (SEM) equipped with a backscattered electron (BSE) detector and energy dispersive X-ray (EDX) spectrometry. Thickness and volume fraction of the phases in the samples were analyzed using the image processing software Image J. X-ray diffraction (XRD) was used to characterize the constituent phase(s) of the sample. Thin sections of the specimens were examined in the transmission electron microscope (TEM, JEM 3010 - HR pole piece, JEOL). TEM samples were prepared by means of Focused Ion Beam (FIB) using an *in-situ* lift-out technique.

Measurement of thermoelectric properties was performed for all samples. Plates of $4 \times 4 \times 10$ mm^2 and $\varnothing 6 \times 1$ mm^2 were cut along and perpendicular to the growth direction, respectively. The electrical conductivity (σ) and Seebeck coefficient (S) were measured using the thermoelectric measurement system ZEM-3 in the temperature range from room temperature to 300 °C. The equilibrium phase diagram[17] suggests that the temperature dependent solubility may lead to microstructural changes during aforementioned measurement of the thermoelectric properties. For assuring the accumulated annealing effect (heating rate 1.5 K/min) during measurement on microstructure and properties, repeated measurements on one sample were performed. The measured properties during the second cycle are essentially the same as the first time, indicating the negligible changes within the measurement time. The thermal conductivity (k_{tot}) was calculated from the values of thermal diffusivity (α), density (ρ) and specific heat (C_P) by the relationship $k = \alpha\rho C_P$, where α was measured using a laser flash system (Netzsch LFA-457), ρ was measured by the Archimedes method, and C_P was determined by a combination of the Dulong-Petit law and a differential scanning calorimeter (Netzsch STA-449FA). The measured values fall into the same range and are also consistent with the calculated values by the Dulong-Petit law. For each sample state, 3 samples prepared by the same experimental procedure were characterized with respect to their thermoelectric properties. All samples exhibited similar or identical temperature dependent Seebeck coefficients and thermal diffusivities. A maximum variation of $\pm 12\%$ of the measured electrical conductivity was observed, and average values were finally used in the present work. The variation of the measured heat capacities and thermal conductivities was $\pm 5\%$. The electronic contribution to the thermal conductivity (k_e) is determined from the electrical conductivity utilizing the Wiedemann-Franz law, $k_e = L\sigma T$. From the total thermal conductivity k_{tot}, the electronic contribution (k_e) is subtracted, yielding k_{LB}, the lattice thermal conductivity k_L plus further contributions, particularly the bipolar contribution k_B.

Results and Discussion

Strong anisotropy in structure and thermoelectric properties of layered Bi_2Te_3-In_2Te_3. Figure 2 shows a typical morphology and the corresponding XRD pattern of an ingot after annealing. Over the width of the ingot, there are only a few grains (see Fig. 2(a)), all of them with the (001) plane parallel to the growth axis (see XRD patterns in Fig. 2e,f). The lamellar structures obtained after annealing also exhibit a preferential orientation of the lamellae along the growth direction, as shown in Fig. 2(b). The solidified sample is very sensitive to cleavage along the axis during the cutting process, as shown in Fig. 2(c,d), demonstrating the pronounced crystallographic anisotropy of the samples. The XRD pattern (Fig. 2(e,f)) confirm that the the Bi_2Te_3 grains grow in a preferential orientation perpendicular to the [001] direction. In_2Te_3 peaks also show the anisotropy, considering that all the visible peaks are indexed ($h\,k\,l$) with $k = l$.

Since the samples produced by zone melting and precipitation exhibit pronounced microstructural anisotropy, also anisotropic thermoelectric properties are expected. Figure 3 shows the temperature dependence of the thermoelectric properties of the sample of which the initial In concentration is 7.5 at%In, i.e. BTIT-7.5, for measurement directions parallel (//) and perpendicular ($\perp$) to the crystal growth direction. The electrical conductivity $\sigma_{//}$ is nearly two orders of magnitude higher than $\sigma_\perp$ for the whole temperature range (Fig. 3(a)). This anisotropy in conductivity is dramatically more pronounced than that generally expected for anisotropic single phase Bi_2Te_3, where the electrical conductivity $\sigma_{//}$ is only 3…7 times larger than $\sigma_\perp$[24–26]. For the Seebeck coefficient S, The negative values agree with the n-type transport behavior of Bi_2Te_3[27,28]. The decrease of $|S|_{//}$ with temperature has been assigned to mixed conduction of holes and electrons (bipolar conduction) in this temperature range due to the increasing number of thermally generated holes, considering the narrow band gap of (or below) 130 meV[29]. The bipolar contribution is also the reason for the increasing conductivity with increasing temperature (3a). As opposed to the strong anisotropy in the electrical conductivity, $|S|_\perp$ is only a little smaller than $|S|_{//}$ and exhibits similar temperature dependence. The bright phase in Fig. 2(b) represents the $(Bi, In)_2Te_3$ phase, whose In concentration was measured as ~3 at%, and the black phase represents the In_2Te_3 phase with negligible Bi concentration. More details on the composition distribution across the two phases will be discussed in detail below.

The temperature dependence of the thermal conductivities in both directions is shown in Fig. 3(c). The thermal conductivity in the direction parallel to the growth direction $k_{tot//}$ is higher than $k_{tot\perp}$, reflecting also the anisotropy of the electrical conductivity. However, after subtracting the electronic contribution ($k_e = L\sigma T$) from the total thermal conductivity, the remaining thermal conductivity $k_{LB//}$ becomes smaller than $k_{LB\perp}$. The value of the Lorenz number is not only dependent on charged carrier concentration and temperature, but also can be influenced by quantum well effects, which e.g. occurs in superlattice/quantum well thin film materials[30,31]. An accurate determination of the Lorenz number of all BTIT composites would require considerably more effort,i.e. the determination of temperature dependent charged carrier concentration, effective carrier mass, Fermi level and so on. For the BTIT composites in the present work, the existence of both electrons and holes, especially the anisotropy not only from the Bi_2Te_3 phase but also from the lamellar aligned microstructure, make the determination of the charge carrier concentration a complex issue. In the literature, Lorenz numbers in the range of $1.2\ldots1.4 \times 10^{-8}$ W Ω K^{-2} for a Bi_2Te_3-based superlattice[32] to $1.6\ldots2.0 \times 10^{-8}$ W Ω K^{-2} for single-phase Bi_2Te_3[33–35] have been reported. The value 1.6×10^{-8} W Ω K^{-2}, which is mostly used for composite materials[3,33–35] and is also used in the present work. Besides, Lorenz numbers calculated with the equation: $L = 1.5 + \exp\left[-\frac{|S|}{116}\right]$ and ranging from 1.8 to 2.2 W Ω K^{-2} were also tried out for the calculation of k_{LB}. However, this lead to non-physical negative $k_{LB//}$ values of BTIT-7.5, most likely due to the complex band structure or the complex scattering mechanism in BTIT. According to published work on Bi_2Te_3[36], the pure lattice thermal conductivity in the given temperature range should be inversely proportional to T and thus decrease with temperature. Whereas this may approximately hold for $k_{LB//}$, it is definitively not the case for $k_{LB\perp}$, indicating a bipolar contribution to the thermal conductivity (see discussion below). The figure of merit, $zT = \frac{S^2\sigma T}{k_{tot}}$, in the direction perpendicular to the growth direction is

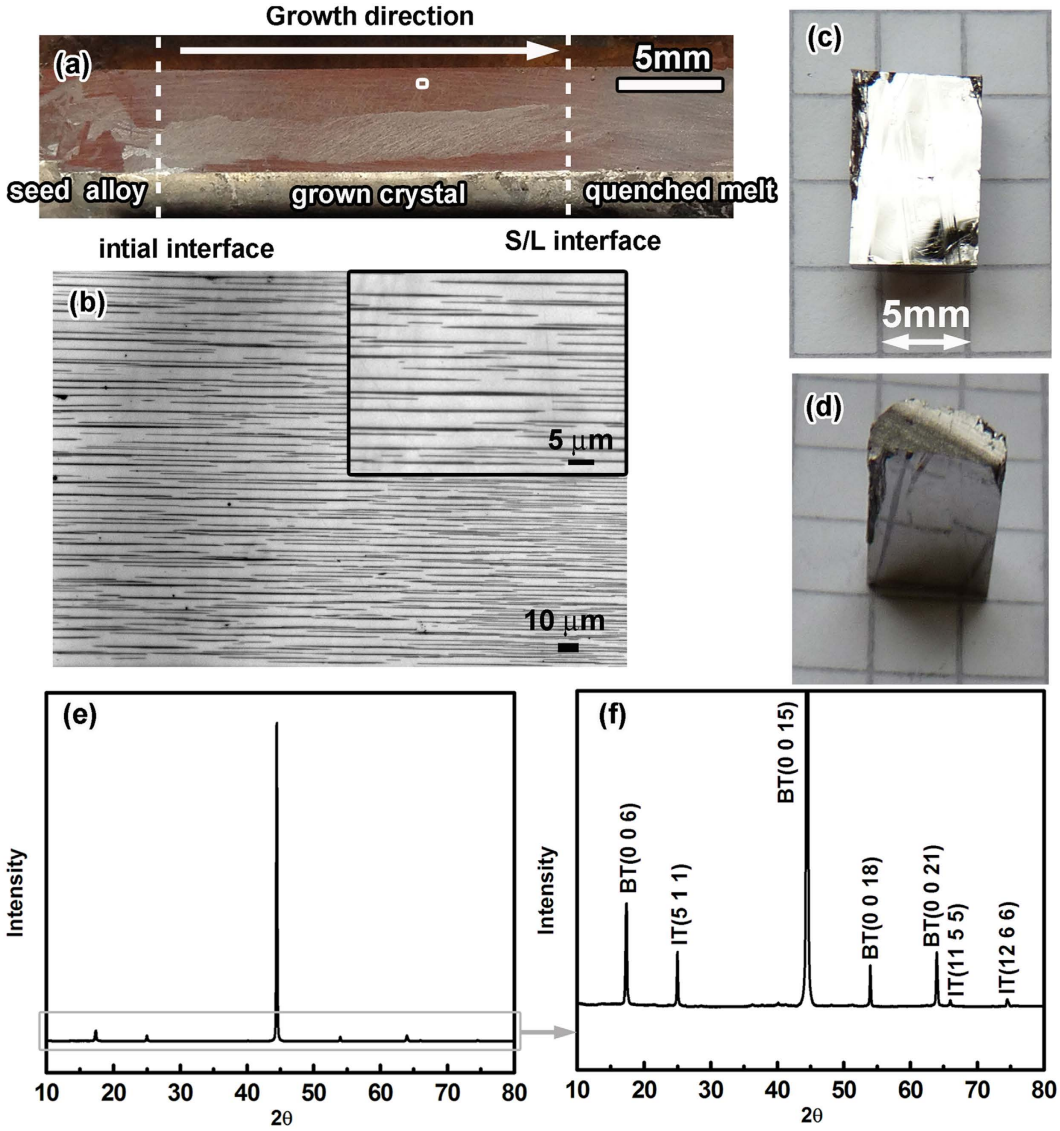

Figure 2. (**a**) Typical macroscopic structure of the Bi-In-Te samples; (**b**) BTIT lamellar structure in a longitudinal section, where the bright phase represents Bi_2Te_3 and the dark phase represents In_2Te_3; (**c,d**) cleaved interface; (**e,f**) XRD patterns.

drastically smaller than in the direction parallel to the growth direction, despite the lower thermal conductivity. This is mainly due to the drastically lower $\sigma_{\perp}$, as shown in Fig. 3(a).

Analytical models of the effective properties of layered Bi_2Te_3-In_2Te_3. When discussing the thermoelectric properties of BTIT, one has to keep in mind that the material is a two-phase composite material (see Fig. 2). Effective medium theory (EMT) and its generalized derivation (GEMT)[37–39] have been used to predict the thermoelectric properties of composite materials where a randomly distributed secondary phase is embedded in a matrix[40,41]. As to BTIT-7.5 in the present work, strong anisotropy effects in structure and thermoelectric properties were confirmed. Hence, it is most appropriate to use a parallel model[42,43] to predict the transport properties along the layer orientation, and a series model[42,43] for the properties perpendicular to the layer orientation. It is worth noting that effects of the interface density are not considered in all these models, which will be shown to be an essential limitation later in the discussion section.

The total Seebeck coefficient (S) as calculated by a mixture rule follows from the Seebeck coefficients of the two phases 1 and 2 by one of the relationships

$$f_1 \frac{\frac{k_1}{S_1} - \frac{k_e}{S_e}}{\frac{k_1}{S_1} + 2\frac{k_e}{S_e}} + f_2 \frac{\frac{k_2}{S_2} - \frac{k_e}{S_e}}{\frac{k_2}{S_2} + 2\frac{k_e}{S_e}} = 0 \quad \text{(EMT model)} \tag{1}$$

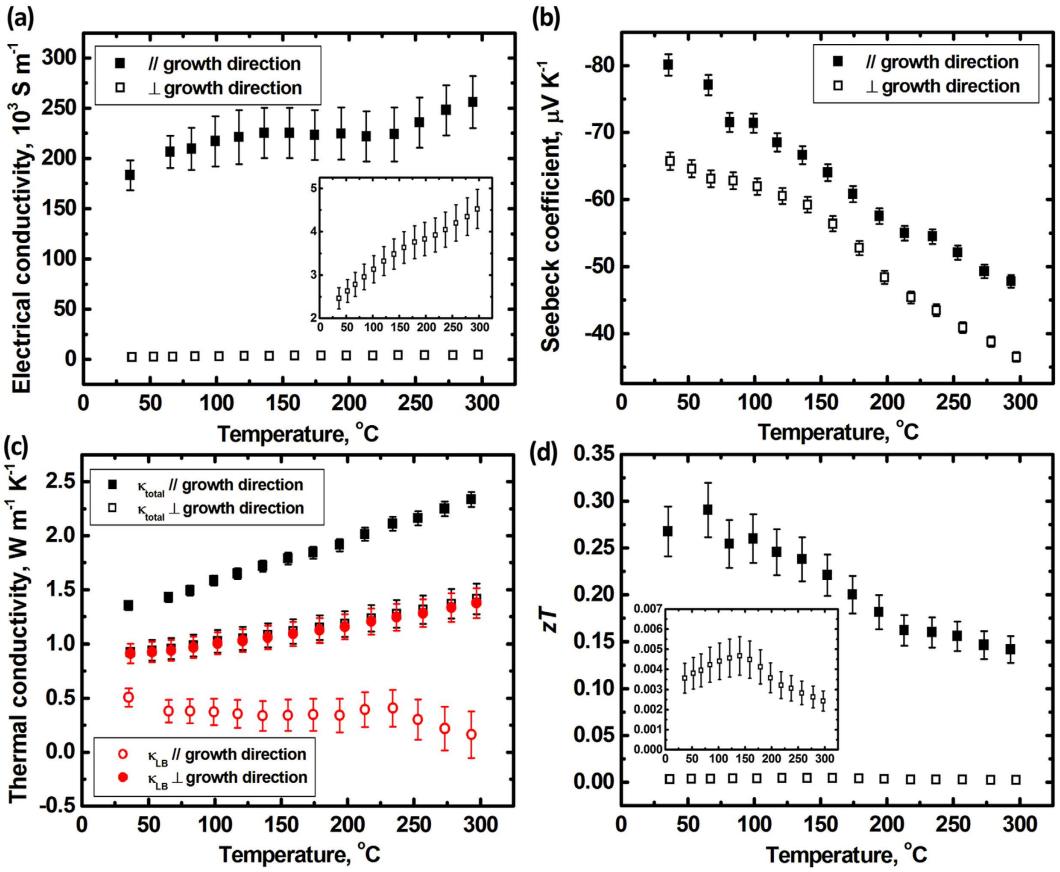

Figure 3. Temperature dependence of (**a**) electrical conductivity σ, (**b**) Seebeck coefficient *S*, (**c**) thermal conductivity *k*, and (**d**) *zT* for BTIT-7.5 in the directions parallel (//) and perpendicular (⊥) to the crystal growth direction. Solid symbols are for parallel (//), open symbols for perpendicular (⊥).

$$f_1\frac{\left(\frac{k_1}{S_1}\right)^{1/t}-\left(\frac{k_e}{S_e}\right)^{1/t}}{\left(\frac{k_1}{S_1}\right)^{1/t}+A\left(\frac{k_e}{S_e}\right)^{1/t}}+f_2\frac{\left(\frac{k_2}{S_2}\right)^{1/t}-\left(\frac{k_e}{S_e}\right)^{1/t}}{\left(\frac{k_2}{S_2}\right)^{1/t}+A\left(\frac{k_e}{S_e}\right)^{1/t}}=0 \text{ (GEMT model)} \tag{2}$$

$$S_{\parallel}=\frac{S_1\sigma_1 f_1+S_2\sigma_2 f_2}{\sigma_1 f_1+\sigma_2 f_2} \text{ (parallel model, upper limit)} \tag{3}$$

$$S_{\perp}=\frac{S_1 k_1 f_1+S_2 k_2 f_2}{k_1 f_1+k_2 f_2} \text{ (series model, lower limit)} \tag{4}$$

and the total electrical conductivity (σ) should be a consequence of the conductivity of the individual phases following

$$f_1\frac{\sigma_1-\sigma_e}{\sigma_1+2\sigma_e}+f_2\frac{\sigma_2-\sigma_e}{\sigma_2+2\sigma_e}=0 \text{ (EMT model)} \tag{5}$$

$$f_1\frac{(\sigma_1)^{1/t}-(\sigma_e)^{1/t}}{(\sigma_1)^{1/t}+A(\sigma_e)^{1/t}}+f_2\frac{(\sigma_2)^{1/t}-(\sigma_e)^{1/t}}{(\sigma_2)^{1/t}+A(\sigma_e)^{1/t}}=0 \text{ (GEMT model)} \tag{6}$$

$$\sigma_{\parallel}=\sigma_1 f_1+\sigma_2 f_2 \text{ (parallel model, upper limit)} \tag{7}$$

$$\sigma_{\perp}=\frac{\sigma_1\sigma_2}{\sigma_2 f_1+\sigma_1 f_2} \text{ (series model, lower limit)} \tag{8}$$

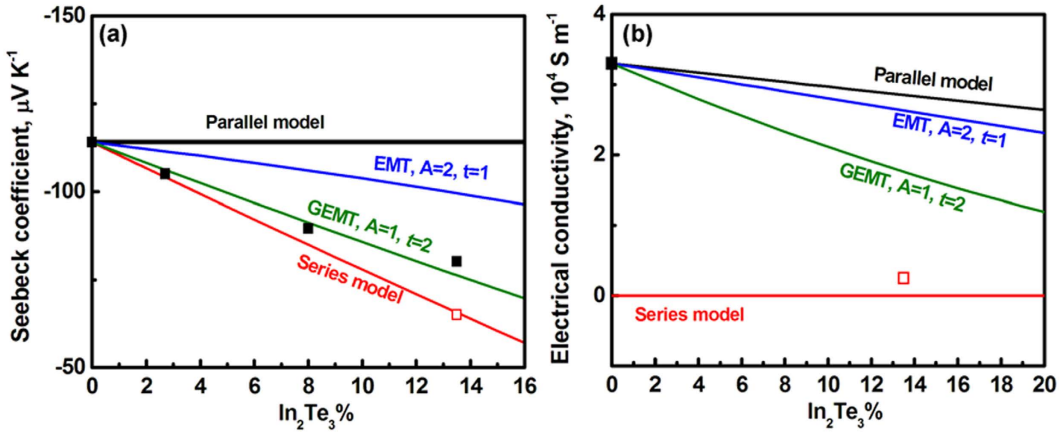

Figure 4. Calculated dependence of room temperature (**a**) Seebeck coefficient and (**b**) electrical conductivity of BTIT on the volume fraction of In_2Te_3.

where f is the volume fraction and k is the total thermal conductivity of the respective constituent phase, A is a constant that depends on the actual percolation threshold φ_c (of phase 2 in phase 1) through the equation $A = (1 - \varphi_c)/\varphi_c$, t is a constant representing the asymmetry of the microstructure, and the subscripts 1, 2 and e refer to Bi_2Te_3, In_2Te_3 and BTIT, respectively[37–39].

Irrespective of the chosen model, the calculated properties of a composite cannot exceed those of one of the constituents. The two phases in our material are substantially different in their thermoelectric properties. Bi_2Te_3 with dissolved In is known to be n-type material for In concentrations ranging from 2…6.5 at%[27,28], with a conductivity in the order of $10^4\ \Omega^{-1}m^{-1}$, In_2Te_3 is a p-type material with a very low conductivity in the order of $10^{-5}\ \Omega^{-1}m^{-1}$[44–46]. Since the In concentration in the Bi_2Te_3 layers of BTIT is ~3at%, the experimental room temperature property values for single phase Bi_2Te_3 with 3at%In, i.e. BT-3, are used for the calculation. A Seebeck coefficient of $-114\,\mu V\ K^{-1}$, an electrical conductivity of $33 \times 10^3\ S\,m^{-1}$, and a thermal conductivity of $1.36\ W\,m^{-1}\,K^{-1}$ are used for the calculation. Since the In_2Te_3 phase in BTIT samples is plate-like with thicknesses of 100…200 nm, the room temperature thermoelectric properties for In_2Te_3 are taken from literature on In_2Te_3 films[44–46]. The Seebeck coefficient for In_2Te_3 is set to $185\,\mu V\ K^{-1}$[44], the electrical conductivity to $5.6 \times 10^{-3}\ S\,m^{-1}$[45], and the thermal conductivity to $1.1\ W\,m^{-1}\ K^{-1}$[46].

When using the EMT or GEMT models to calculate the Seebeck coefficient of BTIT, equations (1) and (2) listed above do not work. The reason is that Bi_2Te_3 is an n-type material with negative Seebeck coefficient, and In_2Te_3 is a p-type material with a positive Seebeck coefficient. Considering the opposite contribution of Bi_2Te_3 and In_2Te_3 to the total Seebeck coefficient of the composite, the EMT/GEMT models need to be adapted, as shown below:

$$f_1 \frac{\frac{k_1}{|S_1|} - \frac{k_e}{S_e}}{\frac{k_1}{|S_1|} + 2\frac{k_e}{S_e}} - f_2 \frac{\frac{k_2}{|S_2|} - \frac{k_e}{S_e}}{\frac{k_2}{|S_2|} + 2\frac{k_e}{S_e}} = 0 \quad \text{(EMT model)} \tag{9}$$

$$f_1 \frac{\left(\frac{k_1}{|S_1|}\right)^{1/t} - \left(\frac{k_e}{S_e}\right)^{1/t}}{\left(\frac{k_1}{|S_1|}\right)^{1/t} + A\left(\frac{k_e}{S_e}\right)^{1/t}} - f_2 \frac{\left(\frac{k_2}{|S_2|}\right)^{1/t} - \left(\frac{k_e}{S_e}\right)^{1/t}}{\left(\frac{k_2}{|S_2|}\right)^{1/t} + A\left(\frac{k_e}{S_e}\right)^{1/t}} = 0 \quad \text{(GEMT model)} \tag{10}$$

The calculation results for the properties of the BTIT composites at room temperature are plotted in Fig. 4 together with the measured values. In the direction perpendicular to the growth direction, the measured properties of BTIT-7.5 are very close to the calculations with the series model. The electrical conductivity in the perpendicular orientation is dominated by In_2Te_3 phase, see eq. (8), i.e. $\sigma_\perp \approx \sigma_{In2Te3}$. BTIT-7.5 exhibits such a low electrical conductivity in the direction perpendicular to the growth direction (Fig. 3(a)). Due to the anisotropic microstructure, the transport properties along the growth direction should follow the parallel model and thus be dominated by the properties of Bi_2Te_3, see eq. (7), i.e. $\sigma_{//} \approx \sigma_{Bi2Te3}$ and eq. (3) $S_{//} \approx S_{Bi2Te3}$. However, the experimentally measured thermoelectric properties in the parallel direction (both $\sigma_{//}$ and $S_{//}$) of BTIT-7.5 divert drastically from the calculated values. The measured $S_{//}$ values are close to the values calculated with the GEMT model ($A = 1$, $t = 2$). All models suggest a decreasing $\sigma_{//}$ with increasing volume fraction of In_2Te_3. However, the large difference between the calculated σ and $\sigma_{//}$ suggest that the Bi_2Te_3/In_2Te_3 interfaces influence the thermoelectric properties in a more complex manner.

Tuning of interface density in Bi_2Te_3-In_2Te_3 via solid state phase transformation. To get deeper insight into the effect of the Bi_2Te_3/In_2Te_3 interfaces on the transport behavior of BTIT, the interface density in

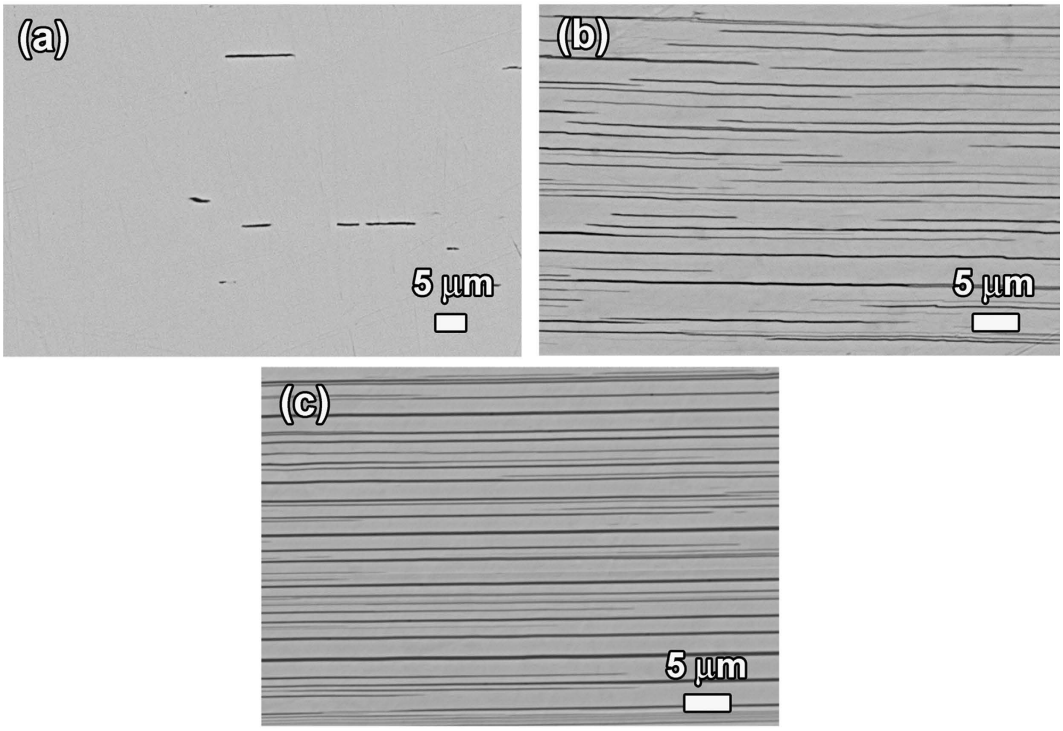

Figure 5. Microstructure of BTIT-c (c = 4, 6, 7.5 at% In), with the dark phase representing In_2Te_3, and the grey phase representing $(Bi,In)_2Te_3$ (~3at%In); (**a**) 4 at%In; (**b**) 6 at%In; (**c**) 7.5 at%In.

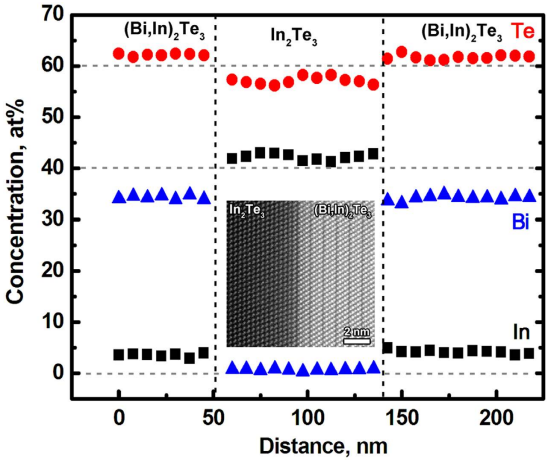

Figure 6. EDX composition analysis in the TEM across $(Bi, In)_2Te_3$ and In_2Te_3 layers; the HRTEM image in the inset illustrates the sharp $(Bi, In)_2Te_3/In_2Te_3$ interface.

BTIT was varied in a controlled way. Since the thermoelectric properties of Bi_2Te_3 are very sensitive to the composition, the Bi_2Te_3/In_2Te_3 interface density was modified by changing the supersaturation of the parent $(Bi, In)_2Te_3$ phase while maintaining the same annealing temperature, i.e. the same composition of each constituent phase. Figure 5 shows cross section microstructures of $(Bi, In)_2Te_3$ (4, 6, and 7.5 at%In) after precipitation annealing at 400 °C. For avoiding projection effects in the lamellar spacing measurements, microstructural analysis was performed in cross sections of the samples. The grey phase in Fig. 5 represents the $(Bi, In)_2Te_3$ phase with an identical In concentration of ~3 at% for all samples, and the black phase represents the In_2Te_3 phase with negligible Bi content. The composition distribution in each phase was determined in the TEM, as shown in Fig. 6. In each phase, the concentration of each element is homogeneous within the measurement scatter of EDX. Interestingly, a slight but significant variation in the Te concentration across Bi_2Te_3/In_2Te_3 interfaces is observed. The concentration of Te in the $(Bi, In)_2Te_3$ phase is a little higher than 60 at%, while the Te concentration in the In_2Te_3 phase is somewhat lower than 60 at%. Inhomogeneity and lattice misfit at heterophase interfaces have been demonstrated to cause transport processes across the interface and hence change the thermoelectric

performance. A high resolution TEM image of a Bi_2Te_3/In_2Te_3 interface is also shown in Fig. 6. Together with the EDX analysis, this confirms that there is no diffusion layer and that the Bi_2Te_3/In_2Te_3 interface is sharp and coherent. As can be clearly seen from Fig. 5, the volume fraction of In_2Te_3 increases and the lamellar spacing decreases with increasing In concentration. Simultaneously, the length of the In_2Te_3 plates increases. For all samples, the thickness of the In_2Te_3 plates is similar, in the order of ~100 to 200 nm. For BTIT-6, the lamellar spacing ranges from ~500 nm to ~3.5 μm, with the majority of lamellar spacings being in the size class ~1.2 μm. For BTIT-7.5, the lamellar spacing is smaller, ranging from ~200 nm to ~2 μm, and most of the lamellae have a spacing below 1 μm. For verifying that 6 days are enough for reaching thermodynamic equilibrium at 400 °C, we compared the measured lamellar spacing values with the diffusion length, $\delta = \sqrt{2Dt}$, where D is the diffusion coefficient and t is the involved time scale. D is of the order of $10^{-12}\,m^2\,s^{-1}$, as found in previous work on the diffusion of metallic elements in Bi_2Te_3[47–49]. The calculated diffusion length in 6 days is 1440 μm, which is much larger than the observed spacing between neighboring In_2Te_3 precipitates for all BTIT samples. This in turn confirms that the equilibrium state at 400 °C is reached. With the In concentration increasing from 4 to 7.5 at%, the volume fraction of In_2Te_3 after annealing was measured as $1.5 \pm 0.5\%$, $7.3 \pm 1.5\%$ and $13.5 \pm 1.5\%$, respectively. These values are consistent with those calculated by the lever rule based on the solubility of In in Bi_2Te_3 (3at%In at 400 °C) and negligible solubility of Bi in In_2Te_3. In the present work, it can be seen from Fig. 5 that the increase in In_2Te_3 volume fraction mainly comes from the decrease of lamellar spacing rather than the increase in thickness of In_2Te_3.

Correlation between the interface density and thermoelectric properties of Bi_2Te_3-In_2Te_3. To get deeper insight into the physical transport mechanisms, the thermoelectric properties of the solid solution sample (BT-3 at%In) and the composite samples (BTIT-4, -6, -7.5 at%In) were characterized in the temperature range from room temperature to 300 °C, see Fig. 7. Since the thermoelectric properties perpendicular to the growth direction are expected to be technically uninteresting, as shown in Figs 3 and 4, only the properties parallel to the sample axis were studied. All samples exhibit a similar temperature dependence trend of the thermoelectric properties. Negative values of the Seebeck coefficient throughout the whole measured temperature range are found for all samples (Fig. 7(a)), indicating n-type transport behavior. With increasing temperature from room temperature to 300 °C, the absolute value of the Seebeck coefficient $|S|$ decreases, and the electrical conductivity σ increases, indicating mixed conduction or bipolar transport behavior[29]. The BT-3 sample shows the highest $|S|$, but the lowest σ of all samples. With increasing volume fraction of In_2Te_3 and decreasing lamellar spacing, $|S|$ decreases while σ increases. Since the conductivity of In_2Te_3 is much smaller than that of Bi_2Te_3, the increase of σ with increasing In_2Te_3 volume fraction is not straightforward to understand.

For qualitatively analyzing the possible reason for the increasing σ, Hall tests at room temperature were performed on all the samples. The measured Hall coefficients of BTIT at room temperature are given in Table 1. The carrier concentration can be calculated from R_H via the equation $R_H = A/ne$, where A is related to the anisotropy factor of the effective carrier mass and the Fermi energy levels[50]. However, the microstructure/property anisotropy and the existence of two types of material, p-type In_2Te_3 and n-type Bi_2Te_3, (i.e. the coexistence of both holes and electrons) make the accurate determination of A not straightforward. Due to a lack of detailed information, an approximation, $R_H = 1/ne$ is used in our present work. We get qualitative information concerning the increase of the electrical conductivity with increasing BT/IT interface density, as listed in Table 1. The measured carrier concentration does not differ much between the samples. This indicates that the contribution of In_2Te_3 and the BT/IT interfaces to the carrier concentration is negligible. This is partly due to the very low room temperature hole concentration of In_2Te_3, $7.8 \times 10^9 cm^{-3}$, which is nearly 10 orders of magnitude lower than that of BT-3In. The increasing σ of BTIT with increasing In_2Te_3 volume fraction mainly comes from the increasing carrier mobility.

The total thermal conductivity shows a non-uniform trend: BTIT-4 and BTIT-6 exhibit a lower k_{tot} than BT-3, and BTIT-7.5 exhibits a comparable k_{tot} as BT-3, as shown in Fig. 7(d). After subtracting the electronic contribution, the thermal conductivity shows a clear trend in Fig. 7(e) – it distinctly decreases with increasing In_2Te_3 fraction. The remaining thermal conductivity after subtracting the electronic contribution contains the lattice thermal conductivity and the bipolar contribution. The pure lattice thermal conductivity should decrease with increasing temperature due to phonon-phonon interaction[36]. In contrast, the bipolar contribution increases due to the increasing number of electron/hole pairs. Thus, all samples show a significant bipolar contribution to the thermal conductivity (Fig. 7(e)), in agreement with the mixed conduction behavior of the Seebeck coefficient and the electrical conductivity. Nevertheless, k_{LB} decreases with increasing In_2Te_3 fraction, and for BTIT-7.5 the overall temperature dependence is inverted from increasing to decreasing (Fig. 7(e)). This indicates the suppression of the bipolar contribution by a decreasing BTIT lamellar spacing. Bipolar transport contributions are counterproductive for the thermoelectric properties, because they do not only increase the thermal conductivity, but also lower the Seebeck coefficient. Thus, BTIT-7.5 with the lowest bipolar contribution has the highest zT value, see Fig. 7(f).

n-Bi_2Te_3/p-In_2Te_3 hetero-interface effects. The enhanced zT values of BTIT are mainly attributed to the increased electrical conductivity and the resulting higher power factor. Bergman and Levy[51] theoretically predicted the possibility of higher thermoelectric power factors than the power factors of the pure components in a composite consisting of two phases, especially for a parallel slabs microstructure. They pointed out that the zT value of a composite can never be beyond the highest value of one of the constituent components[51]. An enhancement of both power factor and thermoelectric figure of merit beyond those of the components in a two-phase composite were first experimentally found in SiGe-Si nanocomposites[52,53]. This enhancement is mainly attributed to a higher carrier mobility, which in turn is interpreted to be induced by inhomogeneous doping only in Si nanograins instead of uniform doping in both components[52]. Selective doping will certainly contribute to the

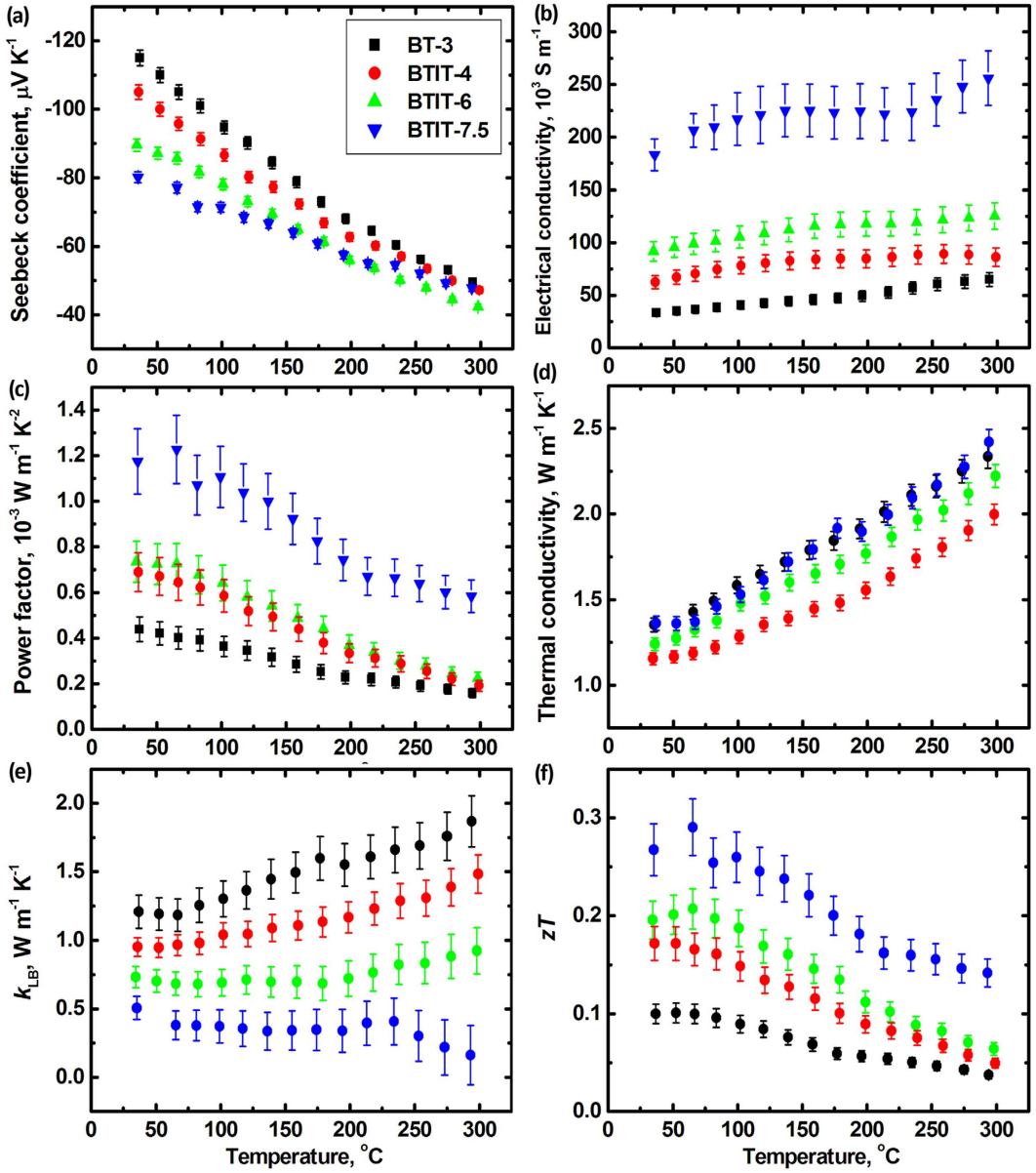

Figure 7. Temperature dependence of Seebeck coefficient S (**a**), electrical conductivity σ (**b**), power factor (**c**), thermal conductivity k_{tot} (**d**), $k_{tot} - k_{LB}$ (**e**), and zT (**f**) of BT-3 and BTIT-4, -6, -7.5.

Sample	R_H (10^{-6} m^{3}A^{-1}s^{-1})	σ (10^3 S m^{-1})	n (10^{19} cm^{-3})	μ (cm^{2}V^{-1} s^{-1})
BT-3In	−0.52	33	1.20	172
BTIT-4In	−0.59	62.5	1.12	368
BTIT-6In	−0.63	92	1.0	580
BTIT-7.5In	−0.55	175	1.13	963

Table 1. Carrier concentration (n) and mobility (μ) of the samples at room temperature (295 K).

band engineering at the interface and may lead to charge transfer from one phase to the other one, which in turn can enhance zT[53].

In the present work, the enhanced electrical conductivity (as a consequence of the higher carrier mobility, see Table 1) is the main reason for enhanced power factor and zT. As for SiGe-Si[52,53], band alignment and charge transfer across Bi_2Te_3/In_2Te_3 interface was considered to be one of the possible reasons. A simple schematic illustration of the band diagram for an n-type $(Bi,In)_2Te_3$/p-In_2Te_3 interface is proposed in the present work, see Fig. 8, in which the maximum work function for In_2Te_3 and the minimum work function for Bi_2Te_3 are used. For p-type In_2Te_3, an electron affinity of 3.85 eV and a band gap of ~1.12 eV have been reported[54]. It is not straightforward

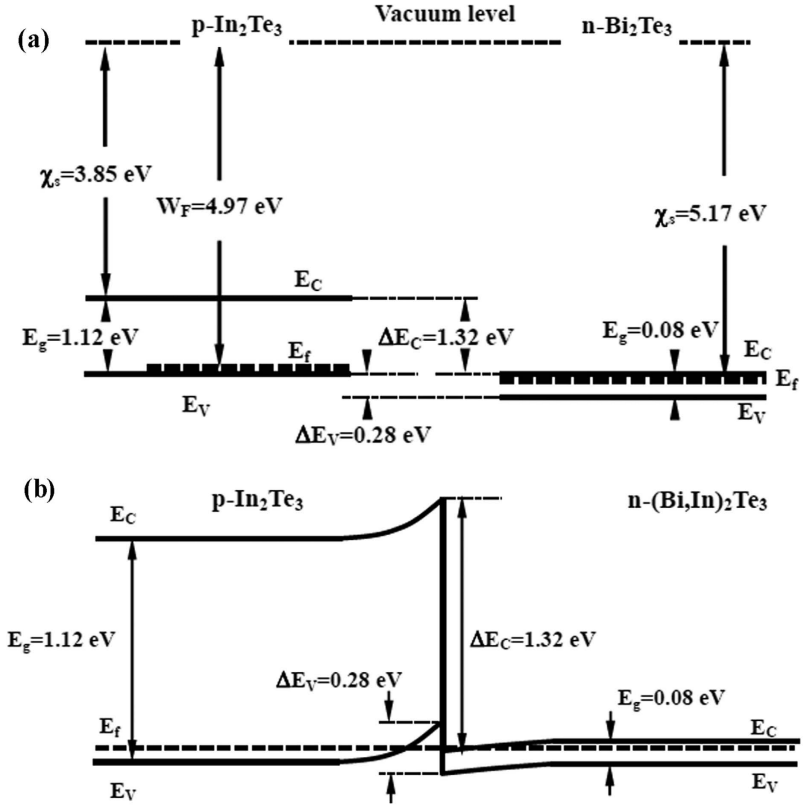

Figure 8. Schematic illustration of (**a**) band diagrams of Bi_2Te_3 and In_2Te_3 phase and (**b**) band bending at Bi_2Te_3/In_2Te_3 interface. E_g: band gap; E_C: conduction band; E_V: valence band; E_f: Fermi level; W_F: working function; χ_s: electron affinity; ΔE_C: offset of conduction band; ΔE_V: offset of valence band.

to determine the Fermi level of In_2Te_3 in BTIT in the present work. In view of the p-type behavior, we assume a Fermi level close to the valence band. Then the work function (W_F) for In_2Te_3 ranges from 4.41 to 4.97 eV. As to n-type Bi_2Te_3 with 3 at% In, so far the band structure is not known and cannot be determined on the basis of the results in our present work. The recently reported band gap value, 0.08 eV, for Bi_2Te_3 with 4 at% In[55] was used in the present work. We assumed a same electron affinity (5.17 eV[56]) as Bi_2Te_3. Considering the n-type transport behavior of $(Bi,In)_2Te_3$, a Fermi level at the same position of the conduction band is used. Even though the Fermi level of In_2Te_3 is higher than that of $(Bi,In)_2Te_3$ at the $(Bi,In)_2Te_3/In_2Te_3$ interface, the electrons tend to flow from In_2Te_3 to $(Bi,In)_2Te_3$ to balance the Fermi level at the contact, which in turns yields band bending. $(Bi,In)_2Te_3$ then can be expected to act as electron acceptor, and the formation of an electron accumulation layer close to the interface to In_2Te_3 can be safely assumed.

The Fermi levels of the two phases and the band offsets are crucial in the band alignment at the interface and the resulting charge transfer between the two phases. Experimentally, alloying/doping in each phase can induce a change of the Fermi level of each phase, and a change in the resulting band offset between the two phases. Moreover, thinking of the difference in the crystal structures of two phases, the lattice misfit and the resulting strain at the two-phase interface can affect the band alignment and then resulting charge transfer across the interface. These factors will lead to different band alignments and final properties[53]. Only suitable doping can lead to good band alignment to ensure the desired charge transfer from one phase to another[53,57], which is an opportunity for enhanced zT values.

In the present case, electron transfer across the BT/IT interface could lead to a change in the thermoelectric properties of the two phases, similarly as for the SiGe-Si nanocomposites[52,53]. Calculations with the properties of the single separated phases $(Bi,In)_2Te_3$ and In_2Te_3 would necessarily lead to a deviation from the experimental data. With a modified charge distribution in the two components and thus a different electrical resistance of each phase, the enhancement of the conductivity of BTIT could probably be explained using the model in ref. 52. Our own simulation calculations suggest an accumulation layer that can also be regarded as a highly conductive third phase. Then, a three-phase model is more realistic for predicting the final properties. In this case, the highly conductive third phase leads to the increasing electrical conductivity with increasing Bi_2Te_3/In_2Te_3 interface density.

Band alignment at hetero-interfaces is regarded as one of the main reasons for enhanced electrical conductivity in two-phase nanocomposites, for example SiGe-Si[52,53] and ZnO:Al – ZnS thin films[58]. As shown in Fig. 8, band bending at the Bi_2Te_3/In_2Te_3 interface may shift the Fermi level closer to the conduction band or even below the Fermi level (metal-like behavior). Such a metal-like surface state of Bi_2Te_3 may also be a possible reason for the increase of electrical conductivity with increasing BT/IT interface density. Together with the metal-like behavior at the BT/IT interfaces, a metal-like surface state of Bi_2Te_3 as a prominent example for a topological insulator[59,60]

may be another possible reason for the increase of electrical conductivity with increasing BT/IT interface density. Besides, In_2Te_3 was reported to exhibit a high room temperature charge carrier mobility, particularly a hole mobility of 1820 cm^2V^{-1} s^{-1} and electron mobility of 2890 cm^2V^{-1} s^{-1}. Previous work on Cu_2Se-CuAgSe[61] indicates that the carrier mobility in each constituent phase plays a critical role for the electrical conductivity of the composite, especially when there is a big difference in the carrier mobility values between the phases.

Tentative Density Functional Theory (DFT) calculations with VASP (see e.g. ref. 62,63) using the Perdew-Burke-Ernzerhof[64] exchange-correlation functional for a supercell built to reproduce the coherent BT/IT interface also predicted the possibility of a metal-like interface state. A crystallographic orientation between Bi_2Te_3 and In_2Te_3 of $<\bar{2}11>_{IT}$ // $<1\bar{1}00>_{BT}$ and $\{111\}_{IT}$//$\{0001\}_{BT}$[65] and an adjusted band off-set as in Fig. 8 were used. Metallic states localized on the Te atoms and on the neighboring In and Bi planes directly at the interface were observed. Generally, an extremely high carrier mobility in the vicinity of the interface is expected. The metal-like layer in the present work extends over a few atomic layers, which is not straightforward to detect experimentally. Metal-like conductivity originating from band alignment and charge transfer through the interface has been found in other systems, for example in $LaAlO_3/SrTiO_3$[66] and SnO/SnO_2[67]. It is worth noting that the band alignment and the resulting formation of a metallic layer at the BT/IT interface is closely related to the band offset between the two phases. The band offset in turn is influenced by alloying/doping and strain in the two phases. These effects are not considered in our reasoning on band alignment and the DFT calculations. However, also in the simplified form they demonstrate the plausibility of the proposed mechanisms.

Conclusions

Metallurgical production methods exhibit high potential for generating high quality thermoelectric materials. In the present work, seeding zone melting and solid state precipitation were applied to produce n-type Bi_2Te_3-In_2Te_3 layered composites of pronounced anisotropy in structure and thermoelectric properties. The spacing of the Bi_2Te_3/In_2Te_3 layers and density of Bi_2Te_3/In_2Te_3 interfaces was tuned via the initial composition of the solid solution samples. Correlations between thermoelectric performance and microstructure were established. With increasing interface density, an increase in electrical conductivity and a decrease of bipolar transport properties lead to a substantial enhancement of zT. The enhanced electrical conductivity is likely to be due to band alignment and charge transfer across Bi_2Te_3/In_2Te_3 interface. The experimental strategy is promising to lead to pronounced high zT values, if the effect of the interfaces is exploited in combination with doping.

References

1. Böttner, H., Chen, G. & Venkatasubramanian, R. Aspects of thin-film superlattice thermoelectric materials, devices, and applications. *MRS Bulletin* **31,** 211–217 (2006).
2. Venkatasubramanian, R. *et al.* Lattice thermal conductivity reduction and phonon localization like behavior in superlattice structures. *Physical Review B* **61,** 3091–3097 (2000).
3. Venkatasubramanian, R., Siivola, E., Colpitts, T. & O'Quinn, B. Thin-film thermoelectric devices with high room-temperature figures of merit. *Nature* **413,** 597–602 (2001).
4. Poudel, B. *et al.* High-thermoelectric performance of nanostructured bismuth antimony telluride bulk alloys. *Science* **320,** 634–638 (2008).
5. Androulakis, J. *et al.* Spinodal Decomposition and Nucleation and Growth as a Means to Bulk Nanostructured Thermoelectrics: Enhanced performance in $Pb_{1-x}Sn_xTe$-PbS. *J. Am. Chem. Soc.* **129,** 9780–9788 (2007).
6. Minnich, A. J., Dressehaus, M. S., Ren, Z. F. & Chen G. Bulk nanostructured thermoelectric materials: current research and future prospects. *Energy Environ. Sci.* **2,** 466–479 (2009).
7. Heinz, N. A., Ikeda, T., Pei, Y. Z. & Snyder, G. J. Applying quantitative microstructure control in advanced functional composites. *Adv. Funct. Mater.* **24,** 2135–2153 (2014).
8. Yang, L., Chen, Z. G., Hong, M., Han G. & Zou, J. Enhanced Thermoelectric Performance of Nanostructured Bi_2Te_3 through Significant Phonon Scattering. *ACS Appl. Mater. Inter.* **7**, 23694–23699 (2015).
9. Zhang, T. *et al. In Situ* Precipitation of Te Nanoparticles in p-Type BiSbTe and the Effect on Thermoelectric Performance. *ACS Appl. Mater. Inter.* **5**, 3071–3074 (2013).
10. Heremans, J. P., Thrush, C. M. & Morelli. D. T. Thermopower enhancement in PbTe with Pb precipitates. *J. Appl. Phys.* **98,** 063703 (2005).
11. Puneet, P. *et al.* Preferential scattering by interfacial charged defects for enhanced thermoelectric performance in few-layered n-type Bi_2Te_3. *Scientific Reports* **3,** 3212 (2013).
12. Liu, J., Wang, X. & Peng, L. Effect of annealing on thermoelectric properties of eutectic PbTe-Sb_2Te_3 composite with self-assembled lamellar structure. *Intermetallics* **41,** 63–69 (2013).
13. Li, J. Q., Li, L. F., Song, S. H., Liu, F. S. & Ao, W. Q. High thermoelectric performance of GeTe-Ag_8GeTe_6 eutectic composites. *J. Alloys Comp.* **565,** 144–147 (2013).
14. Chen, C. L., Lee, J.-G., Arakawa, K. & Mori, H. Quantitative analysis on size dependence of eutectic temperature of alloy nanoparticles in the Ag-Pb system. *Appl. Phys. Lett.* **98,** 083108 (2011).
15. Wu, H. J., Chen, S. W., Ikeda, T. & Snyder, G. J. Formation of ordered nano-wire microstructures in thermoelectric Pb-Ag-Sb-Te. *Acta Mater.* **60,** 1129–1138 (2012).
16. Ikeda, T. *et al.* G.J. Self-Assembled nanometer lamellae of thermoelectric PbTe and Sb_2Te_3 with epitaxy-like interfaces. *Chem. Mater.* **19,** 763–767 (2007).
17. Heinz, N. A., Ikeda, T. & Snyder, G. J. Formation of highly oriented large nanoscale In_2Te_3 precipitates in bulk Bi_2Te_3. *Acta Mater.* **60,** 4461–4467 (2012).
18. Pei, Y. Z., Falk, J. L., Toberer, E. S., Medlin, D. L. & Snyder, G. J. High thermoelectric performance in PbTe due to large nanoscale Ag_2Te precipitates and La doping. *Adv. Funct. Mater.* **21,** 241–249 (2011).
19. Girard, S. N. *et al.* Analysis of phase separation in high performance PbTe–PbS thermoelectric materials. *Adv. Funct. Mater.* **23,** 747–757 (2013).
20. Gorsse, S., Pereira, P. B., Decourt, R. & Sellier, E. Microstructure engineering design for thermoelectric materials: an approach to minimize thermal diffusivity. *Chem. Mater.* **22,** 988–993 (2010).
21. Gorsse, S. *et al.* Nanostructuration via solid state transformation as a strategy for improving the thermoelectric efficiency of PbTe alloys. *Acta Mater.* **59,** 7425–7437 (2011).
22. Liu, D. M., Engelhardt, H., Li, X. Z., Löffler, A. & Rettenmayr, M. Growth of an oriented $Bi_{40-x}In_xTe_{60}$ (x = 3, 7) thermoelectric material by seeding zone melting for the enhancement of chemical homogeneity. *CrystEngComm* **17,** 3076–3081 (2015).

23. Scherpereel, L. R., Palumbo, P. L. & Peretti, E. A. The quasibinary system In_2Te_3-Bi_2Te_3. *J. Less-Common Metals* **14,** 41–46 (1968).
24. Abdullaev, N. A., Kakhramanov, S. Sh., Kerimova, T. G., Mustafayeva, K. M. & Nemov, S. A. Conductivity anisotropy in the doped Bi_2Te_3 single crystals. *Semiconductors* **43,** 145–151 (2009).
25. Yamashita, O. & Sugihara S. High-performance bismuth-telluride compounds with highly stable thermoelectric figure of merit. *J. Mater. Sci.* **40,** 6439–6444 (2005).
26. Hu, L. P. *et al.* Tuning multiscale microstructures to enhance thermoelectric performance of n-type bismuth-telluride-based solid solutions. *Adv. Energy Mater*. **5,** 1500411 (2015).
27. Jansa, L., LošŤák, P., Šrámková, J. & Horák, J. The change of the electric conductivity type in crystals of $Bi_{2-x}In_xTe_3$ solid solutions. *J. Mater. Sci.* **27,** 6062–6066(1992).
28. Karamazov, S., LošŤák, P., Horák, J. & Kužel, R. Point defects in $Bi_{2-x}In_xTe_3$ single crystal. *Phys. Stat. Sol.* (*a*) **148,** 229–237 (1995).
29. Goldsmid, H. The electrical conductivity and thermoelectric power of bismuth telluride. *J. Proc. Phys, Soc.* **71,** 633–646 (1958).
30. Hinsche, N. F.; Mertig, I. & Zahn, P. Lorenz function of Bi_2Te_3/Sb_2Te_3 superlattices. *Journal of Electronic Materials* **42,** 1406–1410 (2013).
31. Kim, Hyun-Sik; Gibbs, Zachary M.; Tang, Y., Wang, H. & Snyder, G. J. Characterization of Lorenz number with Seebeck coefficient measurement. *APL Materials* **3,** 041506 (2015).
32. Beyer, H. *et al.* High thermoelectric figure of merit ZT in PbTe and Bi_2Te_3-based superlattices by a reduction of the thermal conductivity. *Physica E* **13,** 965–968 (2002).
33. Yan, X. *et al.* Experimental studies on anisotropic thermoelectric properties and structures of n-Type $Bi_2Te_{2.7}Se_{0.3}$. *Nano Lett.* **10,** 3373–3378 (2010).
34. Zhang, Y. *et al.* A mesoporous anisotropic n-type Bi_2Te_3 monolith with low thermal conductivity as an efficient thermoelectric material. *Adv. Mater.* **24,** 5065–5070 (2012).
35. Cui, J. L. *et al.* Thermoelectric properties of Cu-doped n-type $(Bi_2Te_3)_{0.9}$-$(Bi_{2-x}Cu_xSe_3)_{0.1}$(x = 0–0.2) alloys. *J. Solid State Chem.* **180,** 3583–3587 (2007).
36. Leibfried, G. & Schlomann Heat conduction in electrically insulating crystals. *Nach. Akad. Wiss. Gottingen. Math. Phys. Klasse*. **2a,** 71 (1954).
37. Sonntag, J. Disordered electronic systems. II. Phase separation and the metal-insulator transition in metal-metalloid alloys. *Phys. Rev. B: Condens. Matter Mater. Phys*. **71,** 115114 (2005).
38. Sonntag, J. Disordered electronic systems. III. Thermoelectric power in alloys with phase separation. *Phys. Rev. B: Condens. Matter Mater. Phys*. **73,** 175703 (2006).
39. Sonntag, J. Thermoelectric power in alloys with phase separation (composites). *J. Phys.: Condens. Matter* **21,** 175703 (2009).
40. Gelbstein, Y. Thermoelectric power and structural properties in two-phase Sn/SnTe alloys. *Journal of Applied Physics*. **105,** 023713 (2009).
41. Vaney, J. B. *et al.* Effective medium theory based modeling of the thermoelectric properties of composites: comparison between predictions and experiments in the glass–crystal composite system $Si_{10}As_{15}Te_{75}$–$Bi_{0.4}Sb_{1.6}Te_3$. *J. Mater. Chem. C* **3,** 11090–11098 (2015).
42. Ashby, M. F. & Brechet, Y. J. M. Designing hybrid materials. *Acta Mater.* **51,** 5801–5821 (2003).
43. Wang, M. & Pan, N. Predictions of effective physical properties of complex multiphase materials. *Mater. Sci. Eng. R* **63,** 1–30 (2008).
44. Lakshminarayana, D., Patel, P. B., Desai, R. R. & Panchal, C. J. Investigation of thermoelectric power in indium sesquitelluride(In_2Te_3) thin films. *J. Mater. Sci.: Materials in electronics* **13,** 27–30 (2002).
45. Mathur, P. C., Kumar, A., Taneja, O. P. & Dawar, A. L. Growth and electrical transport properties of In_2Te_3 thin films. *Thin Solid Films* **78,** 377–383 (1981).
46. Madelung, O., Rössler, U. & Schulz, M. *Ternary Compounds, Organic Semiconductors*; 1st ed, Springer, Heidelberg (2000).
47. Keys, J. D. & Dutton, H. M. Diffusion and solid solubility of gold in single-crystal bismuth telluride. *Journal of Applied Physics* **34,** 1830–1831 (1963).
48. Carlson, R. O. Anisotropic diffusion of copper into bismuth telluride. *J. Phys. Chem. Solids* **13,** 65–60 (1960).
49. Keys, J. D. & Dutton, H. M. Diffusion and solid solubility of silver in single-crystal bismuth telluride. *J. Phys. Chem. Solids* **24,** 563–571 (1963).
50. Lee, H. A theoretical model of thermoelectric transport properties for electrons and phonons. *Journal of ELECTRONIC MATERIALS* **45,** 1115–1141 (2016).
51. Bergman, D. J. & Fel, L. G. Enhancement of thermoelectric power factor in composite thermoelectrics. *Journal of Applied physics* **85,** 8205–8216 (1999).
52. Zebarjadi, M. *et al.* Power factor enhancement by modulation doping in bulk nanocomposites. *Nano Lett.* **11,** 2225–2230 (2011).
53. Yu. B. *et al.* Enhancement of thermoelectric properties by modulation-doping in silicon germanium alloy nanocomposites. *Nano Lett.* **12,** 2077–2082 (2012).
54. Sen, S. & Bose, D. N. Schottky barriers on single crystal indium telluride. *Solid-State Electrons* **26,** 757–759 (1983).
55. Heinz, N. A. Microstructure control and iodine doping of bismuth telluride. *Thesis, California Institute of Technology* (2014).
56. Haneman, D. J. Photoelectric emission and work functions of InSb, GaAs, Bi_2Te_3 and germanium. *Phys. Chem. Solids* **11,** 205–214 (1959).
57. Zebarjadi M., Esfarjani K., Dresselhaus, M. S., Ren Z. F. & Chen G. Perspectives on thermoelectrics: from fundamentals to device applications. *Energy Environ. Sci.* **5,** 5147–5162 (2011).
58. Homm, G. Effects of interface morphology and geometry on the thermoelectric properties of artificially structured ZnO-based thin-films. *Thesis, Justus-Liebig-Universität Giessen* (2012).
59. Zhang, H. *et al.* High-performance bismuth-telluride compounds with highly stable thermoelectric figure of merit. *Nature Physics* **5,** 438–442 (2009).
60. Chen, Y. *et al.* Experimental Realization of a Three-Dimensional Topological insulator, Bi_2Te_3. *Science* **325,** 178–181 (2009).
61. Day, T. W. *et al.* Determining conductivity and mobility values of individual components in multiphase composite $Cu_{1.97}Ag_{0.03}Se$. *Applied Physics Letters* **105,** 172103 (2014).
62. Kresse, G. & Furthmüller, J. Efficiency of ab-initio total energy calculations for metals and semiconductors using a plane-wave basis set. *Comput. Mater. Sci.* **6,** 15–20 (1996).
63. Kresse, G. & Furthmüller, J. Efficient iterative schemes for ab initio total-energy calculations using a plane-wave basis set. *Phys. Rev. B* **54,** 11169 (1996).
64. Perdew, J. P., Burke, K. & Ernzerhof, M. Generalized gradient approximation made simple. *Phys. Rev. Lett.* **77,** 3865–3868 (1996).
65. Liu, D. M. *et al.* Anisotropic n-Type Bi_2Te_3–In_2Te_3 thermoelectric material produced by seeding zone melting and solid state transformation. *Cryst. Growth Des.* **16,** 617–624 (2016).
66. Yoshimatsu, K., Yasuhara, R., Kumigashira, H. & Oshima, M. Origin of Metallic States at the Heterointerface between the Band Insulators $LaAlO_3$ and $SrTiO_3$. *Phys. Rev. Lett.* **101,** 026802 (2008).
67. Albar, A., Wang, Z., Alshareef, H. N. & Schwingenschloegl, U. Formation of Metallic States between Insulating SnO and SnO_2. *Advanced Materials Interfaces* **3,** 1500334 (2016).

Acknowledgements
The authors would like to thank Julia Stötzel and Franziska Maculewicz at Institute of Technology for Nanostructures and CENIDE, University of Duisburg-Essen, Germany, for the help with the thermoelectric property measurement, and Martin Drüe and Martin Seyring at Otto Schott Institute of Materials Research, Friedrich Schiller University Jena, Germany, for the help with the TEM analysis. Financial support by the German Research Foundation (Deutsche Forschungsgemeinschaft DFG) under grant Re1261/15-1 is gratefully acknowledged.

Author Contributions
Markus Rettenmayr and Dongmei Liu conceived and initiated the study. Dongmei Liu and Xinzhong Li prepared all the samples and measured all the thermoelectric data. Roland Schmechel provided access to the temperature dependent thermoelectric characterization facilities. Pedro de Castro Borlido and Silvana Botti performed the DFT calculations. All the authors analyzed the data and wrote the manuscript.

Additional Information
Competing Interests: The authors declare no competing financial interests.

How to cite this article: Liu, D. *et al.* Anisotropic layered Bi_2Te_3-In_2Te_3 composites: control of interface density for tuning of thermoelectric properties. *Sci. Rep.* **7**, 43611; doi: 10.1038/srep43611 (2017).

Publisher's note: Springer Nature remains neutral with regard to jurisdictional claims in published maps and institutional affiliations.